Oceanologia (2015) 57, 116–131

Available online at www.sciencedirect.com

ScienceDirect

journal homepage: www.elsevier.com/locate/oceano

ORIGINAL RESEARCH ARTICLE

Modelling the water and heat balances of the Mediterranean Sea using a two-basin model and available meteorological, hydrological, and ocean data☆

Mohamed Shaltout [a,b,*], **Anders Omstedt** [b]

[a] *Department of Oceanography, University of Alexandria, Faculty of Science, Alexandria, Egypt*
[b] *Department of Earth Sciences, University of Gothenburg, Goteborg, Sweden*

Received 27 October 2014; accepted 6 November 2014
Available online 22 November 2014

KEYWORDS
Mediterranean Sea;
Water budget;
Heat budget;
Gibraltar Strait;
Sicily Channel;
Climate change

Summary This paper presents a two-basin model of the water and heat balances of the Western and Eastern Mediterranean sub-basins (WMB and EMB, respectively) over the 1958–2010 period using available meteorological and hydrological data. The results indicate that the simulated temperature and salinity in both studied Mediterranean sub-basins closely follow the reanalysed data. In addition, simulated surface water in the EMB had a higher mean temperature (by approximately 1.6°C) and was more saline (by approximately 0.87 g kg^{-1}) than in the WMB over the studied period. The net evaporation over the EMB (1.52 mm day^{-1}) was approximately 1.7 times greater than over the WMB (0.88 mm day^{-1}). The water balance of the Mediterranean Sea was controlled by net inflow through the Gibraltar Strait and Sicily Channel, the net evaporation rate and freshwater input. The heat balance simulations indicated that the heat loss from the water body was nearly balanced by the solar radiation to the water body, resulting in a net export (import) of approximately 13 (11) W m^{-2} of heat from the WMB (to the EMB).

☆ This research was undertaken when Dr. Mohamed Shaltout was a visiting scientist at the Ocean Climate Group, Department of Earth Sciences, University of Gothenburg, Sweden. The work is a contribution to the GEWEX/BALTEX phase II and the newly formed programme "Baltic Earth-Earth System Science for the Baltic Sea region" and the HyMex program.
* Corresponding author at: Department of Oceanography, University of Alexandria, Faculty of Science, Moharrem Bey, 21151, Alexandria, Egypt. Tel.:+2 01121501764, fax: +2 033911794.
E-mail address: mohamed.shaltot@alexu.edu.eg (M. Shaltout).
Peer review under the responsibility of Institute of Oceanology of the Polish Academy of Sciences.

ELSEVIER Production and hosting by Elsevier

http://dx.doi.org/10.1016/j.oceano.2014.11.001

1. Introduction

The Mediterranean Sea comprises a series of connected sub-basins with connections to the Atlantic Ocean and Black Sea (Shaltout and Omstedt, 2014). Many oceanographers use the box model concept to describe the oceanic characteristics of the Mediterranean Sea. Tziperman and Speer (1994), for example, used a three-box model to study the thermohaline seasonal cycle of the Mediterranean Sea. The three boxes in this model are arranged and connected vertically as surface, middle, and deep boxes. Bethoux and Gentili (1999) used a 20-box model of heat and water fluxes between boxes to capture the increasing temperature and salinity trends in the Mediterranean Sea. This 20-box model treated the Mediterranean Sea as eight main sub-basins, each divided into several boxes according to their maximum depth (e.g., the Ionian sub-basin is divided into surface, intermediate, deep, and very deep boxes). Elbaz-Poulichet et al. (2001) analysed the input and output fluxes of dissolved metals using a one-box model of the Western Mediterranean sub-basin. They describe the water exchange through the Gibraltar Strait and Sicily Channel using two-layer model exchanges. Matthiesen and Haines (2003) defined a hydrostatically controlled box model to study the Mediterranean Sea's response to post-glacial sea-level rise. This hydrostatic model treated the Mediterranean Sea as one basin comprising three boxes (i.e., the water formation, upper-layer, and lower-layer boxes), connected to the Atlantic Ocean through the Gibraltar Strait. Calmanti et al. (2006) improved a simple model to study the spread of the Mediterranean Sea outflow in the North Atlantic Ocean. This simple model treated the Mediterranean Sea as a single basin but with three vertical boxes connected to the North Atlantic Ocean.

We started analysing the Eastern Mediterranean Sea heat and water balances based on a single-basin ocean modelling approach and using available meteorological, hydrological, and ocean data (Shaltout and Omstedt, 2012). The modelling used a vertically resolved grid with 190 grid cells extending from surface to bottom. We estimated various heat and water components and the net import of approximately 9 W m^{-2} of heat to the Eastern Mediterranean sub-basin from the Western sub-basin. The present paper, our second such heat and water balance study, follows the pattern of the first one but now treats the whole Mediterranean Sea and the modelling approach divides the sea into two coupled sub-basins to study the general oceanic features of each sub-basin. To address the local oceanic features of the Mediterranean Sea, the modelling approach should treat the Mediterranean Sea as 15 sub-basins (Shaltout and Omstedt, 2014). Our process-oriented modelling approach is based on the use of time-dependent models of vertically resolved connected basins, which have been extensively used in the Baltic Sea (for a review, see Omstedt et al., 2014). The approach allows long-term runs on time scales of centuries and millennia to be studied and is a complement to fully three-dimensional model studies. The Mediterranean Sea, which extends from 30°N to 46°N and from 6°W to 36.5°E, has a negative water balance. It is connected to the Atlantic Ocean by the Gibraltar Strait (13 km wide), to the Black Sea by the Bosphorus—Marmara—Dardanelles system, and to the Red Sea by the Suez Canal (Fig. 1). In the present work, we treat the Mediterranean Sea as two coupled sub-basins, i.e., the Eastern Mediterranean sub-basin (EMB) and the Western Mediterranean sub-basin (WMB), connected through the Sicily Channel (149 km wide) and the Strait of Messina (4 km wide) as illustrated in Fig. 1.

Atlantic surface water flows into the Mediterranean Sea through the upper layer of the Gibraltar Strait and mixes with WMB surface water. Part of the surface WMB water then flows through the upper layer of the Sicily Channel to the EMB and mixes with EMB surface water. Net precipitation and river discharge influence the water and heat balances in both sub-basins as well as the exchange with the Black Sea. In the winter, convection occurs because of the negative water balance in certain areas of the northern EMB, forming the deep-water outflow through the Sicily Channel to the WMB (Zervakis et al., 2000). This lower flow together with deep-water formation in the Gulf of Lion (in the northern WMB) is responsible for the dense water outflow through the Gibraltar Strait to the Atlantic Ocean. The Mediterranean Sea's large-scale inverse estuarine circulation is driven by the water balance, causing dense bottom-water formation due to strong evaporation and outflowing dense water through the Sicily Channel and Gibraltar Strait into the Atlantic

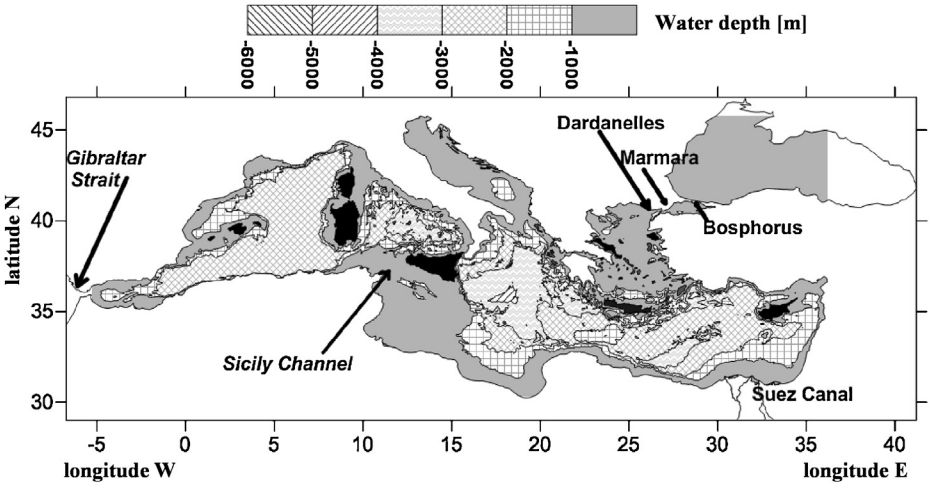

Figure 1 Bathymetric chart of the Mediterranean Sea.

Ocean, with compensating for Atlantic Ocean surface water flowing into the Mediterranean Sea.

The present version of the model uses the PROBE equation solver for the Mediterranean Sea called PROBE-MED version 2.0. PROBE-MED version 2.0 focuses on such processes as diapycnal mixing, inverse estuarine circulation, and land–air–sea interactions in the Mediterranean Sea. The exchange through the Strait of Messina and Suez Canal are neglected as they are smaller than the exchange through the Sicily Channel and Gibraltar Strait. The Black Sea is treated as a river flow into the EMB, as in the earlier study (Shaltout and Omstedt, 2012). Consequently in- and outflows are addressed by the exchange through the Gibraltar Strait and Sicily Channel. The Black Sea together with, in order of declining importance, the Nile, Po, Ceyhan, Adige, Drin, Vjose, Marista, Buyuk Menderes, and Shkumbini rivers are considered the dominant sources of fresh water to the EMB with a combined annual mean discharge of 11,209 $m^3 s^{-1}$. The decreasing freshwater flows from the Black Sea and the River Nile play a significant role in the increasing salinity of the EMB: Black Sea discharge decreased by 9.8×10 $m^3 s^{-1} yr^{-1}$ from 1958 to 2009 due to decreasing net precipitation (Shaltout and Omstedt, 2012; Stanev and Peneva, 2002), while the Nile River discharge was reduced by a factor of more than two after the Aswan high dam was built in 1964 (Ludwig et al., 2009). The Rhone, Ebro, Tiber, Jucar, Cheliff, Moulouya, Mejerdah, and Tafna rivers are considered the dominant sources of fresh water to the WMB with an annual mean discharge of 2811 $m^3 s^{-1}$.

Mediterranean Sea deep water forms in the winter because of evaporation and heat losses. The Adriatic, Aegean, and Levantine sub-basins are the significant sources of EMB deep water (Malanotte-Rizzoli et al., 1999). The enhanced negative water balance in the EMB leads to increased deep-water formation, most pronounced in the Aegean Sea (Zervakis et al., 2000). Since 1969, there has been clear inter-annual variability in deep-water formation in the Gulf of Lion (Mertens and Schott, 1997), which is the main deep water formation area in the WMB (Bethoux et al., 2002). Of the few other deep-water formation areas in the WMB, the main ones are in the Balearic (Salat and Font, 1987) and Ligurian (Sparnocchia et al., 1995) seas.

The water exchange through the Gibraltar Strait is considered a two-layer water flow, surface Atlantic water inflowing to the WMB above a lower outflow from the WMB. This exchange is affected by several factors, such as tides, atmospheric pressure, the steric effect, the geostrophic effect across the Strait, strait bathymetry, and wind (Bormans and Garrett, 1989a,b; Delgado et al., 2001; Menemenlis et al., 2007; Tsimplis and Josey, 2001). Tsimplis and Bryden (2000) estimated the average Atlantic inflow to the Mediterranean basin to be $0.78 \pm 0.17 \times 10^6$ $m^3 s^{-1}$ from 23 January 1997 to 23 April 1997. Garcia-Lafuente et al. (2002) demonstrated that the surface Atlantic flow through the Gibraltar Strait was slightly smaller, i.e., 0.72×10^6 $m^3 s^{-1}$ from 26 October 1997 to 27 March 1998. Soto-Navarro et al. (2010) calculated the surface Atlantic inflow to the Mediterranean Sea through the Gibraltar Strait using observations (2004–2009) to be 0.81×10^6 $m^3 s^{-1}$. Finally, Dubois et al. (2012) presented the results of calculating the Atlantic surface flow through Gibraltar strait over the 1961–1990 period using several models, i.e., the CNRM (Météo-France, Centre National de Recherches Météorologiques), MPI (Max Planck Institute for Meteorology), INGV (Istituto Nazionale di Geofisica e Vulcanologia), LMD (Laboratoire de Météorologie Dynamique), and ENEA (Italian National Agency for New Technologies, Energy and the Environment) models, to be 0.73, 0.75, 0.78, 0.91, and 1.06×10^6 $m^3 s^{-1}$, respectively.

The water exchange through the Sicily Channel can be considered a two-layer baroclinic exchange modified by sea-level variations (Pierini and Rubino, 2001). This exchange has been investigated using CTD data (Astraldi et al., 1999; Stansfield et al., 2002), numerical modelling (Bèranger et al., 2002; Molcard et al., 2002), and sea surface height altimetry data (Shaltout and Omstedt, 2012). Astraldi et al. (1999) calculated the annual average surface flow through the Sicily Channel to be 1.1×10^6 $m^3 s^{-1}$ in the period from November 1993 to October 1997. Bèranger et al. (2002) estimated that the average surface flow over a 13-year period through the Channel was approximately 1.05×10^6 $m^3 s^{-1}$. Molcard et al. (2002) suggested that the transport across the Sicily Channel increases linearly with the actual mean density difference between the basins from 0.3 to 0.8×10^6 $m^3 s^{-1}$. Shaltout and Omstedt (2012) demonstrated that the surface flow through the channel displayed monthly variations with an annual value of 1.16×10^6 $m^3 s^{-1}$ over the 2006–2009 period.

The present paper aims to: (1) study the baroclinic water exchange through the Gibraltar Strait and Sicily Channel and (2) examine the heat and water balances of the WMB and EMB.

2. Material and methods

2.1. Material

The paper uses a two-basin model to estimate the heat and water balances of the WMB and EMB. The model simulates the properties of the two sub-basins based on horizontally averaged advective–diffusive conservation equations for volume, heat, momentum, and salinity, including a two-equation turbulent model, and uses the documented and freely available PROBE equation solver (see Omstedt, 2011). The present model version, PROBE-MED version 2, is freely available from the lead author, including forcing fields. The meteorological input data for PROBE-MED version 2.0 were horizontally averaged using linear interpolation over the two sub-basins. Exchange through the Gibraltar Strait and Sicily Channel was calculated assuming geostrophic baroclinic water exchange. The strength of the approach is that it simply but realistically integrates a large amount of available information extracted from a number of data sources such as:

1. Digitized bathymetric data with a 0.5-min spatial resolution. These data, which were extracted from the British Oceanographic Data Centre and are available via the Centre's website (http://www.bodc.ac.uk/data/onlinedelivery/gebco/), were used to calculate the area/depth distribution of the WMB and EMB.
2. River discharge into the Mediterranean and Black seas was constructed based on data from the Center for Sustainability and the Global Environment (SAGE; available at www.sage.wisc.edu) from 1976 to 1987 together with data from Ludwig et al.'s (2009) river database from 1958 to 2000.

3. Meteorological forcing data, i.e., 2-m height air temperature (°C), zonal/meridional wind speeds at a height of 10 m (m s^{-1}), total cloud cover (0–1), relative humidity (0–1), and total precipitation (m s^{-1}), were obtained from the European Centre for Medium-Range Weather Forecasts (ECMWF; http://data.ecmwf.int/data/) with a 3-h temporal resolution. These data have a spatial resolution of 2.5° × 2.5° from 1958 to 1978 (ERA-40) and 0.75° × 0.75° from 1979 to 2010 (ERA-Interim).
4. Lateral boundary data west of Gibraltar Strait, i.e., daily sea surface temperature (SST; °C) and monthly sea surface salinity (g kg^{-1}), were obtained from three datasets. Daily SST data, 1958–1982, were obtained from the National Center for Environmental Prediction (NCEP) database with nearly a 2° × 2° spatial resolution (http://www.esrl.noaa.gov/psd/data/). Gridded daily AVHRR data (version 2), 1982–2012, with a 0.25° latitude/longitude spatial grid (http://www.ncdc.noaa.gov/oa/climate/research/sst/griddata.php) were used to provide recent SST characteristics. Monthly sea surface salinity data, 1958–1998, with a 1° × 1° spatial resolution were obtained from the National Oceanographic Data Center (NODC; http://www.nodc.noaa.gov).
5. Six variables were used to validate the model results, i.e., evaporation (E), net heat loss from the sea (F_n), solar radiation to the open water surface (F_s^o), total heat loss through the open water surface (F_{loss}), and the vertical sea temperature and salinity profiles of the two sub-basins. Data on E, F_n, F_s^o, and F_{loss} for the WMB and EMB were extracted from the NCEP database. The Mediterranean Data Archaeology (MEDAR) data were used for annual reanalysed temperature and salinity, 1958–2002, with a 0.2° horizontal resolution and vertical resolution, the latter extending from the surface to a depth of 4000 m (Rixen et al., 2005). Reanalysed monthly vertical temperature profiles, 1958–2008, and monthly vertical salinity profiles, 1958–1998, for the two sub-basins were taken from the NODC database (http://www.nodc.noaa.gov).

2.2. Model description

PROBE-MED version 2.0 was designed for analysing the water and heat balances in the WMB and EMB. The modelling approach uses the PROBE general equation solver (Omstedt, 2011; Shaltout and Omstedt, 2012) and couples the two sub-basins using models of the inverse estuarine circulation. The basic model dynamics apply a transient Ekman flow model in each sub-basin with in- and outflows calculating the inverse estuarine circulation. A two-equation turbulent model of the turbulent kinetic energy (k) and its dissipation rate (ε) was used to estimate the turbulence in the surface boundary layer. In the deep layers, the deep-water mixing was parameterized based on the stratification. The turbulent model's initial conditions for the turbulent kinetic energy and its dissipation rate assumed constant and small values. The initial temperature and salinity conditions for the two sub-basins were taken from January 1800 to avoid spin-up calculation errors. The present WMB simulation was forced laterally using Atlantic Ocean surface properties (annual average values of 19°C and 36.85 g kg^{-1}). The model was run from 1800 to 2010 with a vertically resolved 190-cell grid extending from sea surface to sea bottom for a 600-s temporal resolution. In the 1800–1957 period, the model was forced using the average climatic values to reach the equilibrium state, while after 1958, the model was forced using high-time-resolution forcing data. The meteorological data were horizontally averaged using liner interpolation with a 3-h temporal resolution. The 10-m zonal/meridional wind speed, total cloud cover, relative humidity, and total precipitation were used without land correction, while the 2-m air temperature was corrected to reduce the land influence by averaging with the SST (Table 1 shows the annual average values of meteorological forcing data). River discharge was used in the form of monthly mean values.

The full mathematical description of the model is presented by Shaltout and Omstedt (2012); only certain new aspects of the water and heat balance calculations will be presented below.

2.3. Water and heat balances

The water balance equations for the WMB and EMB are formulated using the volume conservation principle as follows:

$$A_{sur,WMB}\frac{\partial \eta_{WMB}}{\partial t} = Q_{in,sur,Gib} - Q_{out,deep,Gib} + Q_{out,deep,Sic} - Q_{in,sur,Sic} + A_{sur,WMB}(P_{WMB} - E_{WMB}) + Q_{f,WMB}, \quad (1)$$

$$A_{sur,EMB}\frac{\partial \eta_{EMB}}{\partial t} = Q_{in,sur,Sic} - Q_{out,deep,Sic} + A_{sur,EMB}(P_{EMB} - E_{EMB}) + Q_{f,EMB}, \quad (2)$$

where the sub-indexes WMB and EMB refer to the two sub-basins. $A_{sur,WMB}$ denotes the surface area of the western sub-basin (i.e., 0.84 × 10^{12} m^2), $A_{sur,EMB}$ denotes the surface area of the eastern sub-basin (i.e., 1.67 × 10^{12} m^2), $\partial\eta/\partial t$ denotes the change in sea level with time and is assumed to be zero for long-term calculations, $Q_{in,sur,Gib}$ denotes the surface flow from the Atlantic Ocean to the WMB through the Gibraltar Strait, $Q_{out,deep,Gib}$ denotes the deep outflow from the WMB to the Atlantic Ocean through the Gibraltar Strait, $Q_{in,sur,Sic}$ denotes the surface flow from the WMB to EMB through the

Table 1 Annual average distribution of meteorological forcing data for the Mediterranean Sea.

	Western Mediterranean sub-basin	Eastern Mediterranean sub-basin
2-m air temperature [°C]	15.14	15.5
10-m zonal wind speed [m s^{-1}]	0.85	1.08
10-m zonal wind speed [m s^{-1}]	−0.76	−1.4
Cloud cover [0–1]	0.34	0.28
Relative humidity [0–1]	0.76	0.73
Precipitation rate [m s^{-1}]	1.73 × 10^{-8}	1.77 × 10^{-8}

Sicily Channel, $Q_{out,deep,Sic}$ denotes the lower outflow from the EMB to WMB through the Sicily Channel, P and E denote the precipitation and evaporation rates, respectively, and Q_f denotes the river discharge to the sub-basin.

The heat balance equation for the WMB/EMB can be formulated based on conservation principles (Omstedt, 2011) as follows:

$$\frac{dH_{WMB}}{dt} = (F_{in,sur,Gib} - F_{out,deep,Gib} + F_{in,deep,Sic} - F_{out,sur,Sic} - F_{loss,WMB})A_{sur,WBM}, \quad (3)$$

$$\frac{dH_{EMB}}{dt} = (F_{in,sur,Sic} - F_{out,deep,Sic} - F_{loss,EMB})A_{sur,EMB}, \quad (4)$$

where H $\left(= \iint \rho C_p T\, dz\, dA\right)$ is the total heat content, ρ is the sea water density, T is the water temperature, and C_p is the heat capacity. F_{in} $(= \rho C_p T_{in} Q_{in}/A_{sur})$ and F_{out} $(= \rho C_p T_{out} Q_{out}/A_{sur})$ are the heat fluxes associated with in- and outflows, respectively, through the Gibraltar Strait and Sicily Channel. T_{in} and T_{out} are the temperatures of in- and outflows through the Gibraltar Strait and Sicily Channel, respectively. F_{loss} is the total heat loss to the atmosphere from each sub-basin (a negative sign indicates that the fluxes go from the atmosphere to the water) and can be calculated from:

$$F_{loss} = F_n + F_s^w, \quad (5)$$

where F_n $(= F_h + F_e + F_l)$ denotes the sum of the turbulent and long-wave heat fluxes at the sea surface, F_h is the sensible heat flux, F_e is the latent heat flux, F_l is the net long-wave radiation, $F_s^w (= F_s(1 - \alpha_W))$ denotes the short-wave radiation penetrating the open water surface in each sub-basin, F_s is the solar radiation to the water surface, and α_W is the surface water albedo.

2.4. Water exchange through the Gibraltar Strait and Sicily Channel

The water exchanges through the Gibraltar Strait and Sicily Channel are both assumed to be baroclinic and geostrophically controlled. The surface flow from Atlantic Ocean into the WMB can then be formulated as a baroclinic geostrophic flow (as has been applied in the Baltic Sea; see Omstedt, 2011; Stigebrandt, 2001) as follows:

$$Q_{in,sur,Gib} = \frac{g\beta\,\Delta S_s}{2f}(H_{sur,Gib})^2, \quad (6)$$

where g is the acceleration of gravity, ΔS_s is the difference in surface salinity between the WMB and Atlantic Ocean, β $(= 8 \times 10^{-4})$ is the salinity contraction coefficient, $H_{sur,Gib}$ is the thickness of the surface layer (set to equal 150 m; Delgado et al., 2001), and f is the Coriolis parameter.

The deep-water flow from the EMB to WMB is calculated from:

$$Q_{out,deep,Sic} = \frac{g\beta\,\Delta S_i}{2f}(H_{sill}^{eff} - H_{sur,Sic})^2, \quad (7)$$

where ΔS_i is the salinity difference in the EMB between the intermediate salinity at the effective sill depth and the surface salinity, H_{sill}^{eff} is the effective depth of the sill between the connected sub-basins (set to equal 500 m), and $H_{sur,Sic}$ is the surface-layer thickness (set to equal 150 m; Shaltout and Omstedt, 2012). The surface inflow from the WMB to EMB and the deep-water outflow from the WMB to Atlantic Ocean are both calculated from volume conservation.

Black Sea outflow water to the Mediterranean Sea is considered a source of fresh water for the EMB. From the Black Sea volume conservation equation, we calculate the net volume input from the Black Sea to the EMB ($Q_{bs,emb}$) according to:

$$Q_{BS,EMB} = A_{sur,BS}(P_{BS} - E_{BS}) + Q_{f,BS}, \quad (8)$$

where the sub-index BS refers to the Black Sea, and $A_{sur,BS}$ is the Black Sea surface area $(4.6 \times 10^8\ m^2)$. Seven significant rivers discharge into the Black Sea, i.e., the Danube, Dnieper, Rioni, Dniester, Kizilirmak, Sakarya, and Southern Bug rivers, with a combined annual average discharge into the Black Sea of 9560 $m^3\ s^{-1}$.

2.5. Statistical validation of model output

Several of the model output data from the PROBE-MED version 2.0 model, such as the sea surface, intermediate-depth, and deep-water properties of temperature and salinity as well as calculated fluxes such as E, F_n, F_s^o, and F_{loss}, were validated using available datasets and two objective dimensionless quality metrics (Edman and Omstedt, 2013; Eilola et al., 2011; Stow et al., 2009).

The first statistical quantity (skill metric) calculated the correlation coefficient (r as defined in Eq. (9)) between the observed and modelled data. The skill metric quantities illustrate how the model results follow the observations.

$$r = \frac{\sum_{i=1}^{n}(P_i - \overline{P})(O_i - \overline{O})}{\sqrt{\sum_{i=1}^{n}(P_i - \overline{P})^2 \sum_{i=1}^{n}(O_i - \overline{O})^2}}, \quad (9)$$

where the number of observations is n, the ith of n observed (modelled) results is denoted $O_i(P_i)$, and the average of observed (modelled) results is denoted $\overline{O}(\overline{P})$.

The second statistical metric (cost function) normalized the bias between the modelled and observed data using the standard deviation (SD) of the observed data.

$$C = \frac{\sum_{i=1}^{n}(P_i - O_i)/SD(O)}{n}. \quad (10)$$

We follow Eilola et al. (2011) and Edman and Omstedt (2013) and classify the values of $C = 0$–1 and $(1 - r) = 0$–$1/3$ as indicating good agreement and strong correlation, the values of $C = 1$–2 and $(1 - r) = 1/3$–$2/3$ as indicating reasonable agreement and moderate correlation, and the values of $C > 2$ and $(1 - r) > 2/3$ as indicating poor agreement and weak or negative correlation.

3. Results

3.1. Water exchange through Gibraltar Strait and Sicily Channel

The baroclinic equations (Eqs. (6) and (7)) and the water balance equations (Eqs. (1) and (2)) were used to model the water exchange through the Gibraltar Strait and Sicily Channel and the results are illustrated in Fig. 2.

Surface and deeper flows through the Gibraltar Strait were calculated and the long-term means were estimated to be $0.65 \times 10^6\ m^3\ s^{-1}$ and $0.63 \times 10^6\ m^3\ s^{-1}$, respectively. The surface and deep flows through the Sicily Channel were

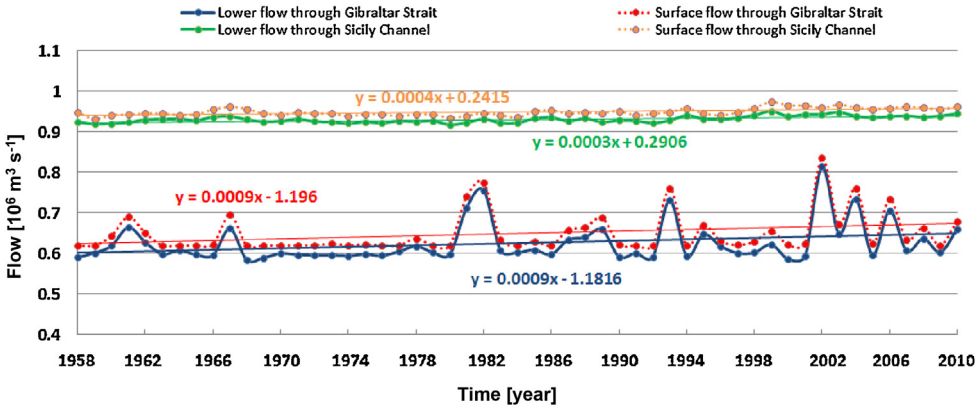

Figure 2 Time series of average annual surface and lower flows through the Gibraltar Strait and Sicily Channel.

calculated as long-term means to be 0.95×10^6 m^3 s^{-1} and 0.93×10^6 m^3 s^{-1}, respectively, almost 40% greater than the Gibraltar Strait flows.

There are clear annual variations in the flows through the Gibraltar Strait but no strong annual variability in the flows through the Sicily Channel. The flows through the Gibraltar Strait and Sicily Channel displayed positive significant trends of 0.0009×10^6 m^3 s^{-1} yr^{-1} and 0.0004×10^6 m^3 s^{-1} yr^{-1}, respectively.

3.2. Validation of the modelled results

The present paper uses various reanalysis datasets instead of direct observations to validate the model results. Reanalysis data give a superior state estimate, produced by combining models with observations covering large spatial and temporal scales. By contrast, observations do not cover the Mediterranean Sea spatial distribution and are valid only over a specific range of times. The current study uses three of the best relevant datasets to validate the modelling results. The NCEP dataset was used to validate weather variables (Jakobson et al., 2012) MEDAR and NODC datasets were used to validate oceanic variables (Rixen et al., 2005; Shaltout and Omstedt, 2012).

Validations of the PROBE-MED version 2.0 model were performed for surface temperature, surface salinity, evaporation, net heat loss, solar radiation, and total heat loss through the two sub-basins. Fig. 3 classifies the results by dividing the statistics into three fields: an inner field (good

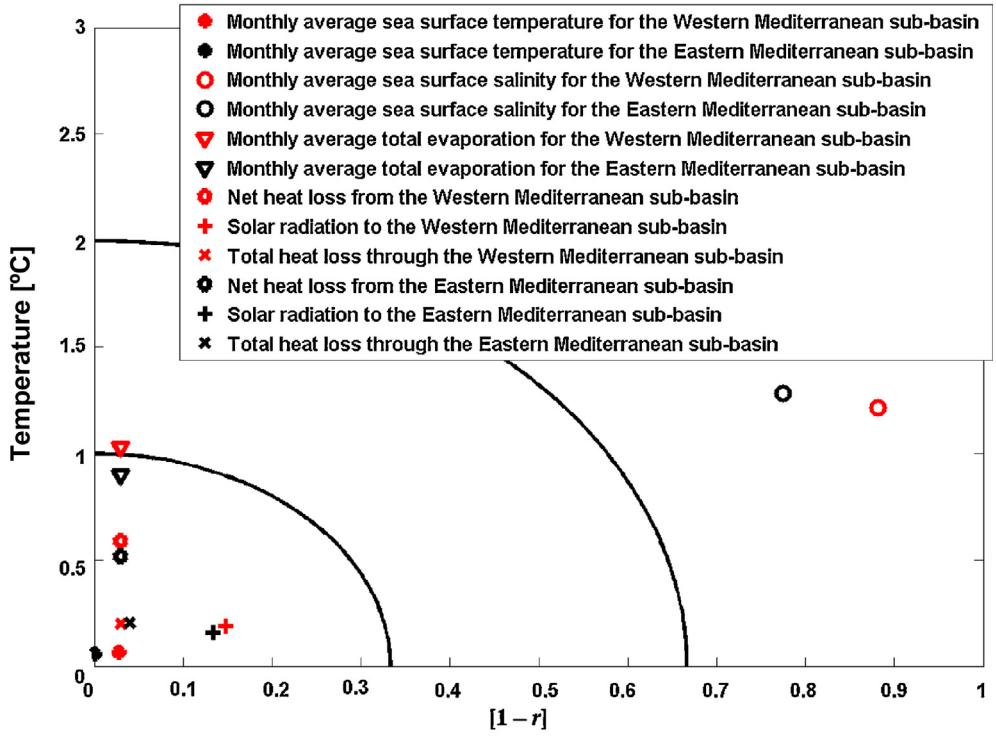

Figure 3 The dimensionless quality metrics r (the correlation coefficient) and C (the volume-weighted mean of the cost function) of the Mediterranean Sea, 1963–2002. Red (black) represents the Western (Eastern) Mediterranean sub-basin. The inner field represents good agreement, the middle field reasonable agreement, and the outer field poor agreement. (For interpretation of the references to colour in this figure legend, the reader is referred to the web version of the article.)

agreement between reanalysed and modelled results), middle field (reasonable agreement between reanalysed and modelled results), and outer field (poor agreement between reanalysed and modelled results).

In both the WMB and EMB, five of the six studied parameters are well modelled. However, monthly average sea surface salinities are not modelled satisfactorily over the two studied sub-basins (Fig. 3). There is an insignificant bias of

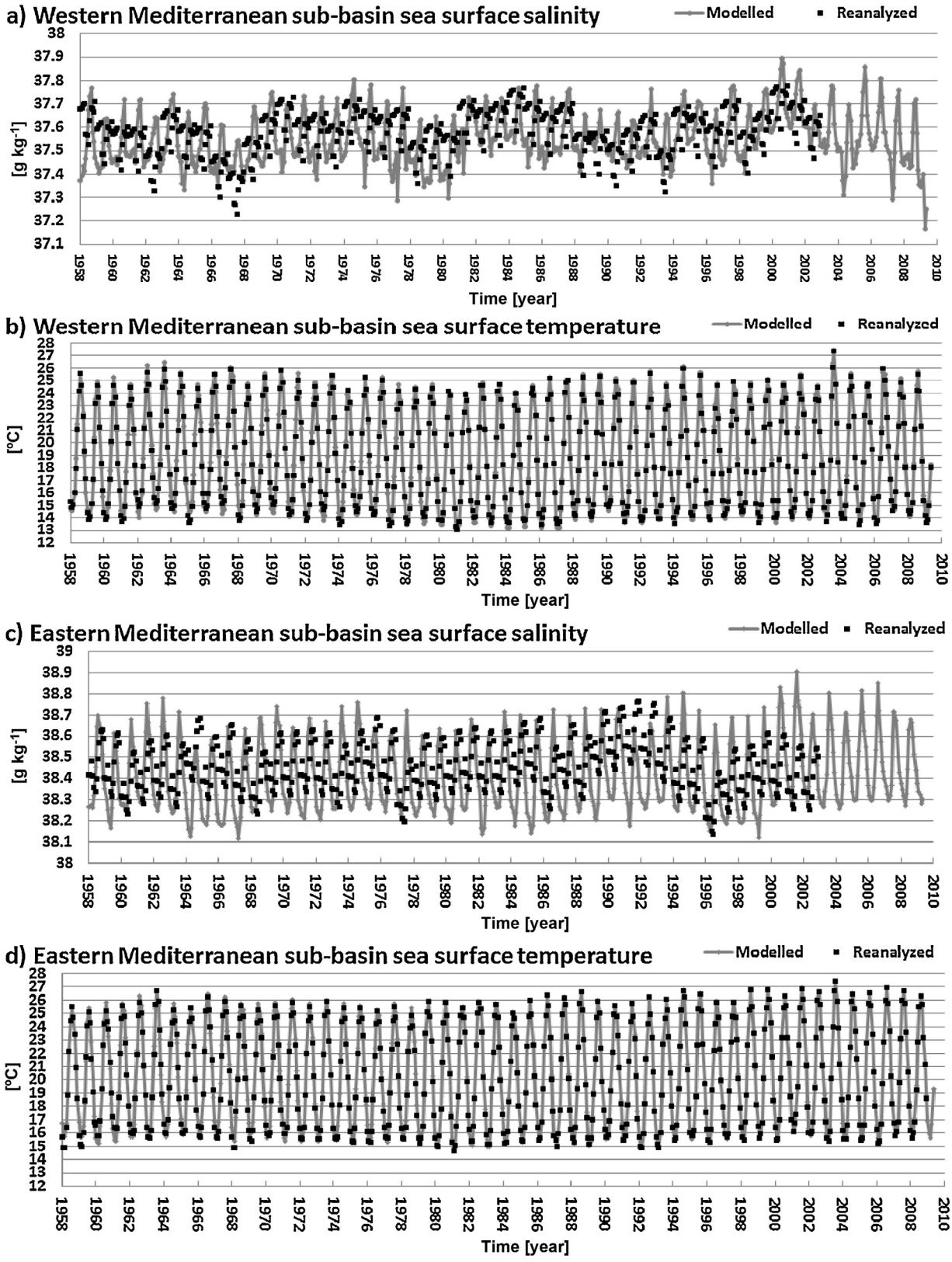

Figure 4 Surface modelled and reanalysed temperatures and salinities in the Eastern and Western Mediterranean sub-basins.

less than 0.2% between the PROBE-MED version 2.0 model calculations and the reanalysed monthly averaged sea surface salinity data, but the resolution of the observed and modelled data differ greatly (see discussion below).

Generally, the PROBE-MED version 2.0 model results for E, F_n, F_s^o, and F_{loss} follow the NCEP reanalysed data closely with an insignificant bias for both studied sub-basins (Fig. 3). NCEP evaporation data were used here as they constituted a dataset independent of the ECMWF datasets used for forcing. This step is considered an important test of the modelled results.

A direct comparison of the modelled monthly SST and salinity data with reanalysed data (from the NODC database) is presented in Fig. 4. The results indicate that PROBE-MED version 2.0 realistically captured the SST and salinity in the WMB and EMB. The bias between the modelled and reanalysed surface temperature is insignificant for both studied sub-basins. However, the modelled surface salinity is lower by approximately 0.09 and 0.11 g kg^{-1} for the WMB and EMB sub-basins, respectively. It is also obvious that the model indicates larger seasonal variations in surface salinity than do the reanalysed data.

The model results were further examined by comparing annual temperatures and salinities for the surface (0–150 m), intermediate (150–600 m), and deep (>600 m) layers with reanalysed MEDAR data (Fig. 5). In the surface layer (0–150 m), the modelled surface temperatures closely follow the reanalysed temperatures with an insignificant bias. However, the modelled surface-layer salinities are lower, especially in the EMB. The modelled long-term mean surface-layer temperatures (salinities) in the WMB and EMB are 14.7°C (37.5 g kg^{-1}) and 16.8°C (38.2 g kg^{-1}), respectively. In the intermediate layer (150–600 m), the modelled temperatures are overestimated while the modelled salinities are underestimated. This is probably because of the horizontal averaging of the forced data for the whole WMB and EMB, which reduced the effect of deep-water convection. In the deep layer (below 600 m), there is a negligible bias between the modelled and reanalysed temperatures and salinities. The variability in the modelled results is less significant than in the reanalysed data simply due to the coarse model resolution. The modelled long-term mean deep-layer temperatures (salinities) were 13.1°C (38.5 g kg^{-1}) and 13.7°C (38.7 g kg^{-1}) for the WMB and EMB, respectively.

3.3. Modelled water budget components for the Western and Eastern Mediterranean sub-basins

The various modelled water components for the 1958–2010 period are presented in Table 2. It can be concluded from the calculations that the in- and outflows through the Sicily Channel are approximately 40% larger than the in- and outflows through the Gibraltar Strait. In general, the net precipitation is approximately three times greater than the river discharge. The total precipitation and net evaporation rates are also larger for the EMB than the WMB. In addition, river runoff to the EMB is approximately four times greater than river runoff to the WMB.

The difference between in- and outflows for the WMB (i.e., $Q_{in,sur,Gib} + Q_{out,deep,Sci} - Q_{out,deep,Gib} - Q_{in,sur,Sci}$) and the EMB (i.e., $Q_{in,sur,Sci} - Q_{out,deep,Sci}$) is of the order of 10^4 m^3 s^{-1}. These net flows for the WMB and EMB are balanced mainly by net precipitation and river discharge. The calculations also indicate that the maximum monthly mean values for $Q_{in,sur,Gib}$ and $Q_{out,deep,Gib}$ occur in February and March, while the maximum monthly mean values for $Q_{in,sur,Sci}$ and $Q_{out,deep,Sci}$ occur in August. The net precipitation reaches its minimum monthly mean value in August for the WMB (-0.021×10^6 m^3 s^{-1}) and the EMB (-0.065×10^6 m^3 s^{-1}). However, the net precipitation reaches its maximum monthly mean value in November for the WMB (-0.003×10^6 m^3 s^{-1}) and in December for the EMB (-0.002×10^6 m^3 s^{-1}). Generally, Q_f for the WMB ranged from 0.002×10^6 m^3 s^{-1} in August to 0.004×10^6 m^3 s^{-1} in February; however, Q_f for the EMB ranged from 0.006×10^6 m^3 s^{-1} in August to 0.018×10^6 m^3 s^{-1} in April.

The annual mean net flow through the WMB is larger than through the EMB (Fig. 6); moreover, the net flows through the WMB and EMB display positive trends of 5.2×10 m^3 s^{-1} yr^{-1} and 3.3×10 m^3 s^{-1} yr^{-1}, respectively. The net precipitation is negative for the Mediterranean Sea, especially over the EMB, indicating that evaporation is larger than precipitation and without any trends. Annual river discharge into the EMB is larger than river discharge into the WMB because we have treated the Black Sea outflow as river input into the EMB. The river discharge displays no trend for the WMB. For the EMB, river discharge decreases by a significant 2.1×10 m^3 s^{-1} yr^{-1}. This reduction is explained by an approximately 50% decrease in River Nile discharge after the building of the Aswan High Dam in 1964 together with decreased freshwater inflow from the Black Sea. The Black Sea water discharge displays a negative trend over the 1958–2009 period (Shaltout and Omstedt, 2012).

Generally, we find no trend in net precipitation over the EMB and WMB, together with no trend in river discharge into the WMB but a significant decrease in river discharge into the EMB. Accordingly, we would expect to find increased salinity in the EMB but not in the WMB. This agrees well also with the earlier findings of Skliris et al. (2007) and Shaltout and Omstedt (2012).

3.4. Modelled heat budget components for the Western and Eastern Mediterranean sub-basins

The climatic monthly mean surface temperatures, salinities, and evaporation rates, 1958–2010, calculated from the PROBE-MED version 2.0 model are presented in Fig. 7. The climatic monthly mean surface temperatures for the WMB (EMB) ranged from 13.8 ± 0.4°C in February (15.5 ± 0.4°C in March) to 25.1 ± 0.7°C in August (26.1 ± 0.6°C in August); the climatic monthly mean surface salinities for the WMB (EMB) ranged from 37.4 ± 0.11 (38.2 ± 0.05) in April to 37.6 ± 0.09 (38.6 ± 0.09) in August; and the climatic monthly mean evaporation rates over the WMB (EMB) ranged from 1.78 ± 0.87 mm day^{-1} in May (2 ± 0.77 mm day^{-1} in April) to 3.03 ± 1.4 mm day^{-1} in November (3.69 ± 1.37 mm day^{-1} in December). In the summer, the surface temperature reaches its maximum values for both studied sub-basins, as do surface salinity and evaporation rate values.

The heat balances for the WMB and EMB are controlled mainly by the net heat loss from the sea ($F_n = F_h + F_e + F_l$), solar radiation to the open water surface (F_s^o), and heat exchange between surrounding sub-basins. Total heat loss through the open water surface (F_{loss}) is the sum of F_s^o and F_n, and the results are presented in Table 3 and Figs. 8 and 9.

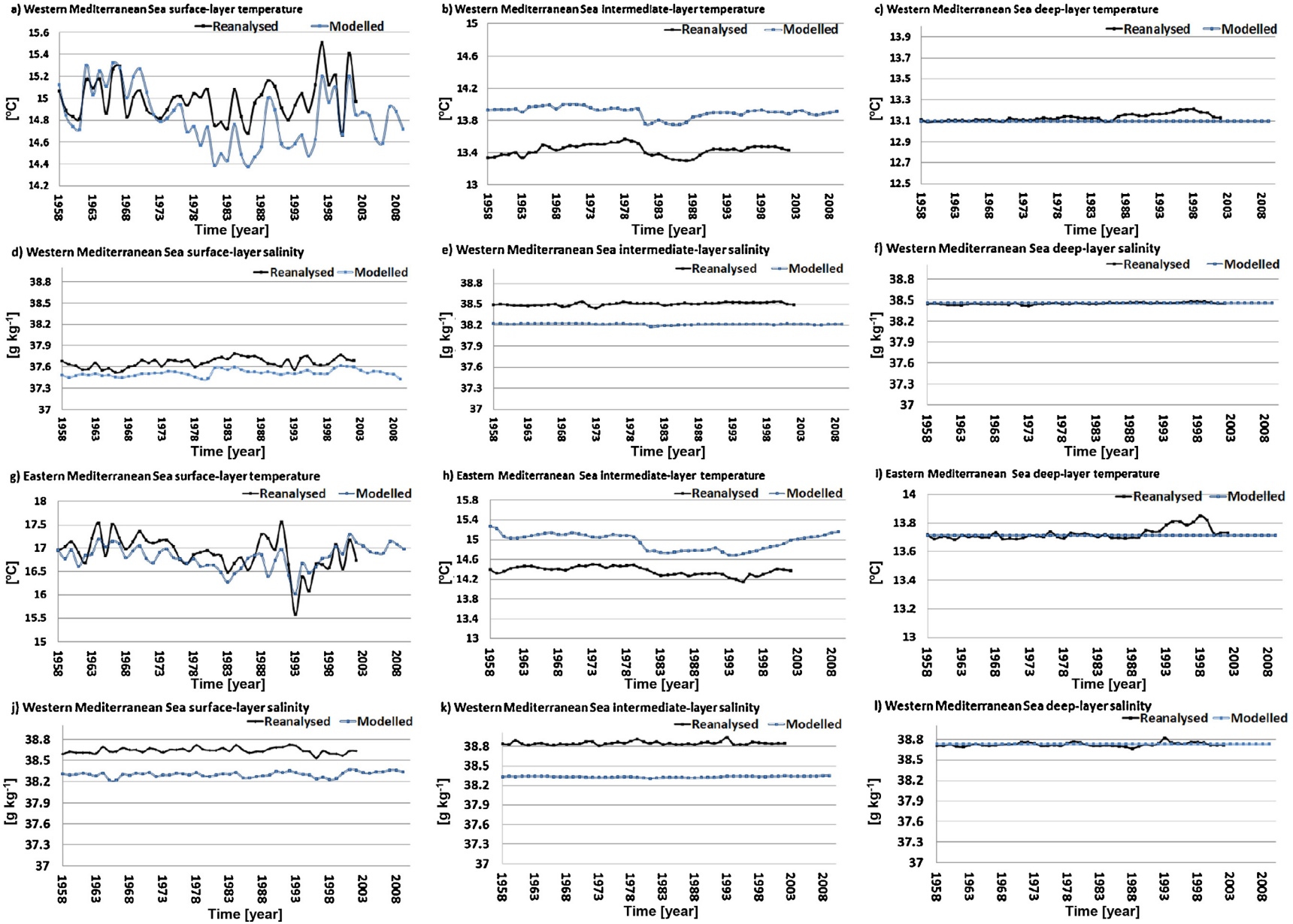

Figure 5 Annual average temperatures and salinities of three different layers of the Western and Eastern Mediterranean sub-basins.

Table 2 Modelled climatic monthly mean water balance for the Western and Eastern Mediterranean sub-basins.

		Q_f [10^6 m^3 s^{-1}]	P [mm day^{-1}]	E [mm day^{-1}]	$A_s(P-E)$ [10^6 m^3 s^{-1}]	$Q_{in,s,g}$ [10^6 m^3 s^{-1}]	$Q_{out,l,g}$ [10^6 m^3 s^{-1}]	$Q_{in,s,s}$ [10^6 m^3 s^{-1}]	$Q_{out,l,s}$ [10^6 m^3 s^{-1}]
Jan.	WMB	0.003	2.061	2.516	−0.004	0.72	0.72	0.84	0.85
	EMB	**0.012**	**3.040**	**3.321**	**−0.005**				
Feb.	WMB	0.004	1.813	2.274	−0.004	**0.74**	**0.74**	0.83	0.84
	EMB	**0.013**	**2.617**	**3.017**	**−0.008**				
Mar.	WMB	0.004	1.400	1.885	−0.005	**0.74**	**0.74**	0.83	0.83
	EMB	**0.015**	**1.652**	**2.299**	**−0.013**				
Apr.	WMB	0.003	1.477	1.891	−0.004	0.63	0.63	0.85	0.85
	EMB	**0.018**	**1.019**	**2.000**	**−0.019**				
May	WMB	0.003	0.950	1.778	−0.008	0.62	0.61	0.92	0.90
	EMB	**0.016**	**0.562**	**2.068**	**−0.029**				
Jun.	WMB	0.003	0.435	1.963	−0.015	0.62	0.57	1.01	0.97
	EMB	**0.011**	**0.272**	**2.652**	**−0.046**				
Jul.	WMB	0.002	0.158	2.232	−0.020	0.62	0.54	1.09	1.03
	EMB	**0.007**	**0.144**	**3.515**	**−0.065**				
Aug.	WMB	0.002	0.328	2.449	−0.021	0.62	0.54	**1.11**	**1.05**
	EMB	**0.006**	**0.217**	**3.594**	**−0.065**				
Sep.	WMB	0.002	1.400	2.756	−0.013	0.62	0.56	1.08	1.03
	EMB	**0.007**	**0.858**	**3.595**	**−0.053**				
Oct.	WMB	0.002	2.220	2.498	−0.003	0.62	0.60	1.01	0.99
	EMB	**0.008**	**1.740**	**3.317**	**−0.030**				
Nov.	WMB	0.003	2.761	3.026	−0.003	0.62	0.61	0.94	0.93
	EMB	**0.010**	**2.779**	**3.589**	**−0.016**				
Dec.	WMB	0.003	2.692	2.974	−0.003	0.63	0.64	0.87	0.88
	EMB	**0.012**	**3.572**	**3.688**	**−0.002**				
Ann.	WMB	0.003	1.451	2.352	−0.009	0.65	0.63	0.95	0.93
	EMB	**0.011**	**1.529**	**3.053**	**−0.029**				

Bold refers to EMB and non-bold refers to WMB.

The latent heat flux (F_e) and long-wave radiation (F_l) are clearly larger fluxes than the sensible heat flux (F_h), as seen in Table 3. In addition, the long-term mean solar radiation to the WMB and EMB is −173.27 W m^{-2} and −192.73 W m^{-2}, respectively, the negative signs indicating fluxes into the water body. Moreover, the average heat loss from the EMB is positive, indicating net heat loss at the surface, and negative for the WMB, indicating net heat gain for the WMB. This is also reflected in the SSTs, which are higher in the EMB than the WMB. The long-term mean value of F_{loss} is negative (−12.66 W m^{-2}, heat gain) for the WMB and positive (10.85 W m^{-2}, heat loss) for the EMB. The latter agrees well with the value of F_{loss} for the EMB previously calculated by Shaltout and Omstedt (2012). The net heat gain and loss for the WMB and EMB need to be balanced by the difference in heat transports through the sub-basins. Moreover, F_{loss} from the two studied sub-basins was negative from March to September, indicating fluxes into the water body. From October to February, however, F_{loss} from the two studied sub-basins was positive, in agreement with previous findings of Shaltout and Omstedt (2012).

In addition, there is no trend in F_n over the two studied sub-basins, but a negative trend in F_s^o indicates an increasing heat gain in the sub-basins (Fig. 9), especially over EMB, probably due to changes in total cloud cover over the study period. The total heat loss displays no net trend for the WMB but a decreasing trend (0.6 W m^{-2} yr^{-1}) for the EMB. The difference between this result for the EMB and the previous finding of Shaltout and Omstedt (2012) is because the current ERA-Interim forcing data used are more accurate (0.75° × 0.75°) than those used previously (1.5° × 1.5°).

The negative value of the annual average F_{loss} (−12.66 W m^{-2}) for the WMB indicates that the WMB exports heat to the connected sub-basin, while the positive value of the annual average F_{loss} (10.85 W m^{-2}) for the EMB indicates that the EMB imports heat from the connected sub-basin. These long-term means can be compared with the rough estimates as follows. Assuming a steady state and averaging over a long period together with Eq. (3) and neglecting heat from rivers, the heat conservation equation can be written as:

$$F_{loss,WMB}A_{sur,WMB} \approx \rho_o C_p(Q_{in,sur,Gib}T_{in,sur,Atl} + Q_{out,deep,Sci}T_{out,deep,EMB}) - \rho_o C_p(Q_{out,deep,Gib}T_{out,deep,WMB} + Q_{in,sur,Sci}T_{in,sur,WMB}),$$

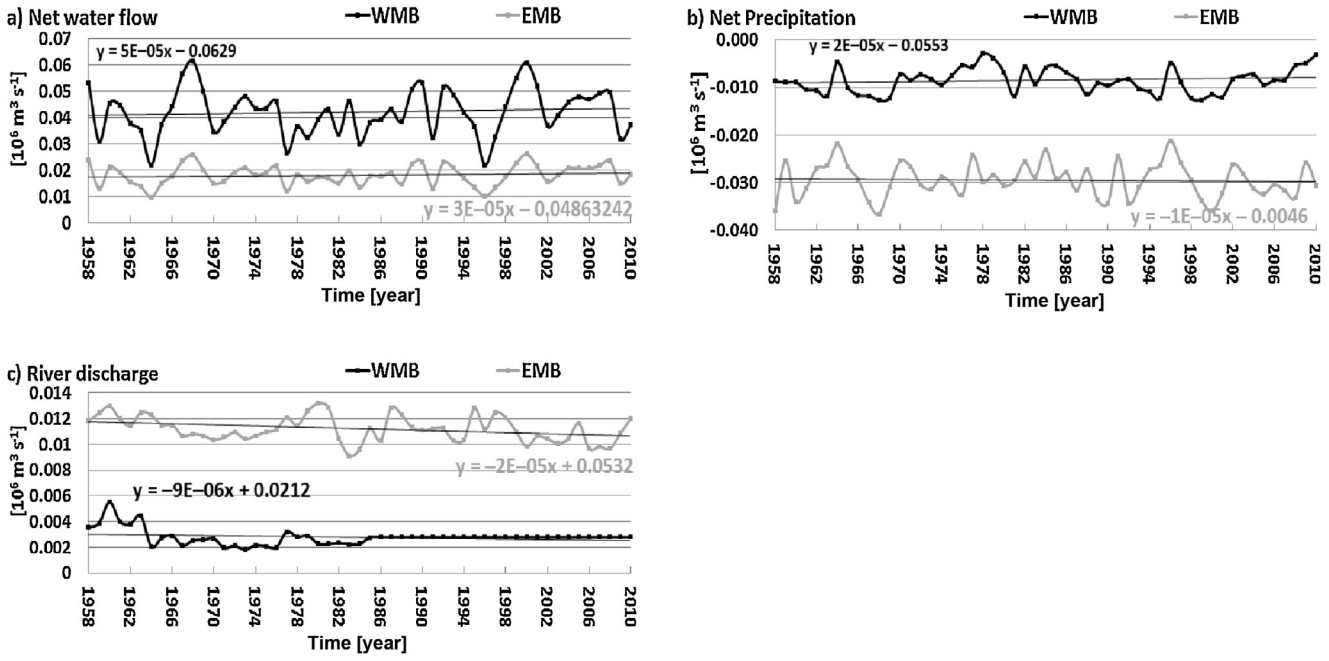

Figure 6 Annual mean modelled water balance components for the Western and Eastern Mediterranean sub-basin water components: (a) net water flow, (b) net precipitation rates, and (c) river discharge.

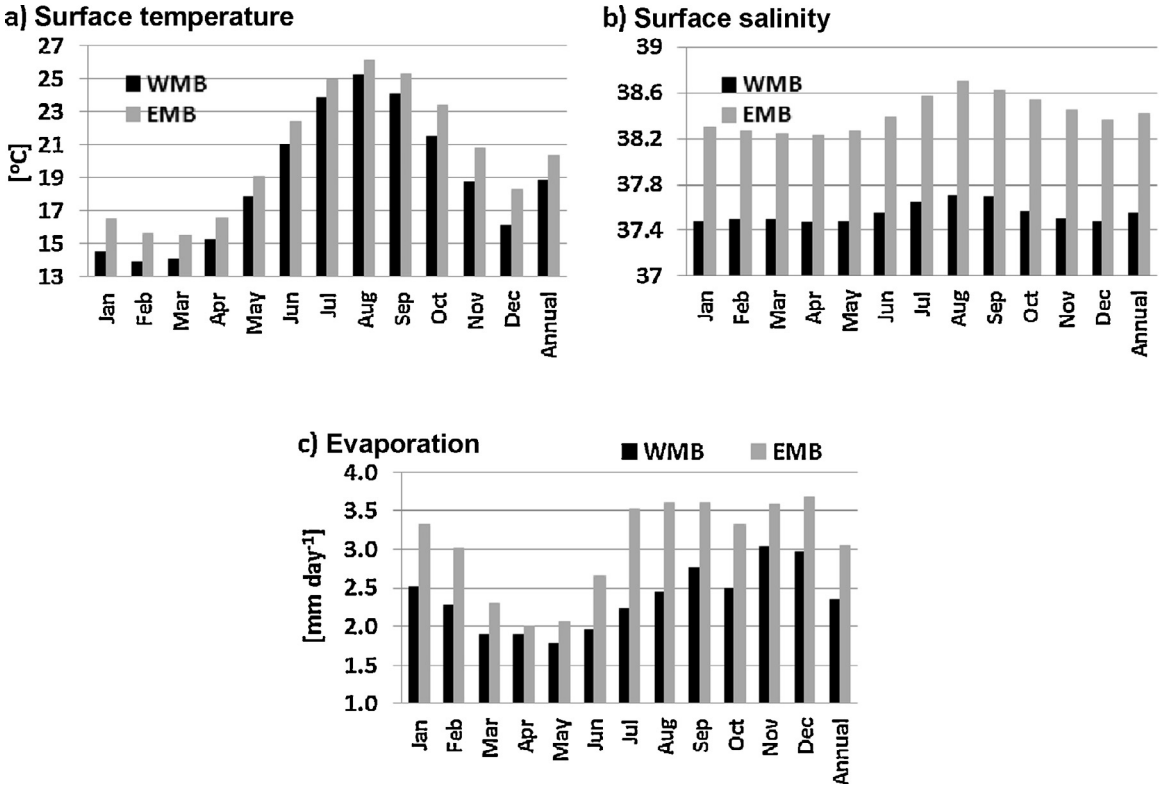

Figure 7 Climate monthly average sea surface temperatures, sea surface salinities, and evaporation rates.

Table 3 Modelled climatic monthly mean heat balance for the Western and Eastern Mediterranean sub-basins.

	F_h [W m^{-2}]		F_e [W m^{-2}]		F_l [W m^{-2}]		F_s^o [W m^{-2}]		F_{loss} [W m^{-2}]	
	WMB	EMB	WMB	EMB	WMB	EMB	WMB	EMB	WMB	EMB
Jan.	29.36	**45.29**	72.80	**96.09**	74.41	**92.77**	−70.74	**−86.83**	105.82	**147.32**
Feb.	25.96	**39.64**	65.80	**87.30**	74.45	**89.49**	−105.60	**−121.62**	60.60	**94.81**
Mar.	18.54	**25.94**	54.55	**66.52**	69.62	**82.12**	−160.22	**−177.22**	−17.51	**−2.63**
Apr.	18.35	**20.62**	54.72	**57.88**	70.93	**81.38**	−212.39	**−229.30**	−68.39	**−69.42**
May	16.20	**19.90**	51.46	**59.83**	71.02	**84.19**	−248.44	**−270.87**	−109.76	**−106.95**
Jun.	15.37	**19.96**	56.80	**76.75**	75.69	**83.68**	−282.54	**−302.55**	−134.68	**−122.16**
Jul.	15.11	**20.99**	64.58	**101.70**	78.66	**79.79**	−293.96	**−305.91**	−135.60	**−103.44**
Aug.	15.13	**20.22**	70.87	**103.99**	76.89	**78.93**	−256.96	**−276.84**	−94.07	**−73.71**
Sep.	15.32	**23.64**	79.73	**104.02**	69.74	**87.76**	−187.89	**−218.12**	−23.09	**−2.70**
Oct.	15.06	**26.31**	72.29	**95.97**	62.37	**89.66**	−118.80	**−146.76**	30.92	**65.18**
Nov.	25.76	**36.33**	87.55	**103.84**	70.43	**92.07**	−76.58	**−96.18**	107.17	**136.06**
Dec.	31.73	**46.37**	86.04	**106.71**	73.97	**94.17**	−60.59	**−76.23**	131.16	**171.02**
Ann.	20.14	**28.79**	68.04	**88.35**	72.43	**86.44**	−173.27	**−192.73**	−12.66	**10.85**

Bold refers to EMB and non-bold refers to WMB.

where T is the sea surface, the sub-index *in* (out) refers to inflow (outflow), *sur* (deep) refers to the surface (deep) layer water, and *Atl* (*Gib*) refers to the Atlantic Ocean (Gibraltar Strait). C_p is the heat capacity, i.e., 4200 J (kg °C)$^{-1}$, and ρ_o is the reference density of sea water, i.e., 10^3 kg m^{-3}.

Then the total heat loss from the WMB ($F_{loss,WMB}$) can then be roughly estimated to be approximately −9 W m^{-2}, which has the same sign but is slightly lower than the value indicated in Table 3 (−12.66 W m^{-2}).

Similarly, the total heat loss (neglecting heat from rivers) from the EMB ($F_{loss,EMB}$) can roughly be written as:

$$F_{loss,EMB}A_{sur,EMB} \approx \rho_o C_p(Q_{in,sur,Sci}T_{in,sur,WMB} - Q_{out,deep,Sci}T_{out,deep,EMB}).$$

The total heat loss from the EMB ($F_{loss,EMB}$) can then be roughly approximately 11 W m^{-2}, which is near the value indicated in Table 3 (10.85 W m^{-2}).

The final test to evaluate the PROBE-MED 2.0 model results was to compare the modelled annual changes in the heat and salt content for the whole WMB/EMB water column with the MEDAR reanalysed data (data not shown). For the WMB, there was a bias in the heat content of approximately 9% but an insignificant bias in the salt content. For the EMB, there was an insignificant bias in the heat content and a bias of 2% in the salt content. Clearly, the PROBE-MED version 2.0 model realistically captures the general water and heat cycles of the Mediterranean Sea as well as the differences between the western and eastern parts of the sea.

3.5. Effect of large-scale atmospheric circulation

The coupling between the large-scale atmospheric circulation and the Mediterranean Sea water balance was examined by analysing the relationship between the winter North Atlantic Oscillation Index (NAOI; extracted from the KNMI climate explorer database, climexp.knmi.nl) and the winter net precipitation (Table 4). The *t*-test was used to examine the significant correlations at a 95% significance level. Table 4 shows a significant inverse correlation between the NAOI and winter net precipitation rates over the WMB. The relationship between the NAOI and WMB evaporation rates is insignificant, but between the NAOI and WMB precipitation is significant. For the EMB, no significant relationships with the NAOI could be found.

The NAOI influences the net precipitation over the WMB and therefore the water balance of the Mediterranean Sea. This agrees with the previous findings of Philandras et al. (2011), who stated that the precipitation over the Mediterranean region is inversely correlated with NAOI, especially in the western and northern regions.

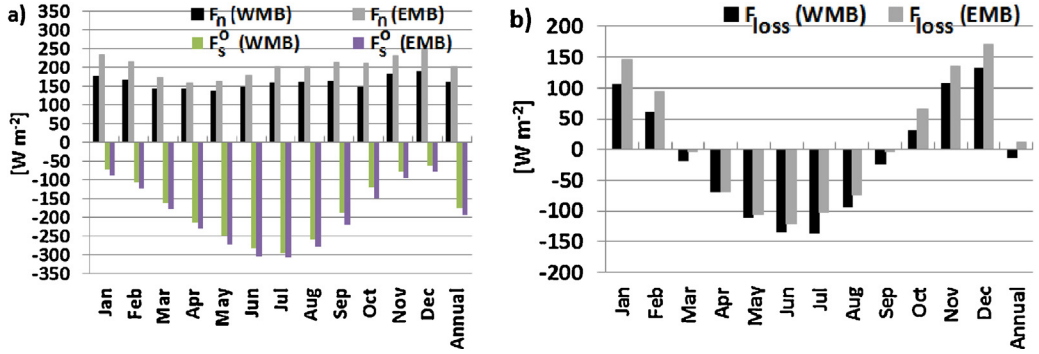

Figure 8 Modelled climatic monthly mean heat fluxes for the Eastern and Western Mediterranean sub-basins: (a) net heat loss from the sea (F_n) together with solar radiation to the open water surface (F_s^o) and (b) total heat loss through the open water surface (F_{loss}).

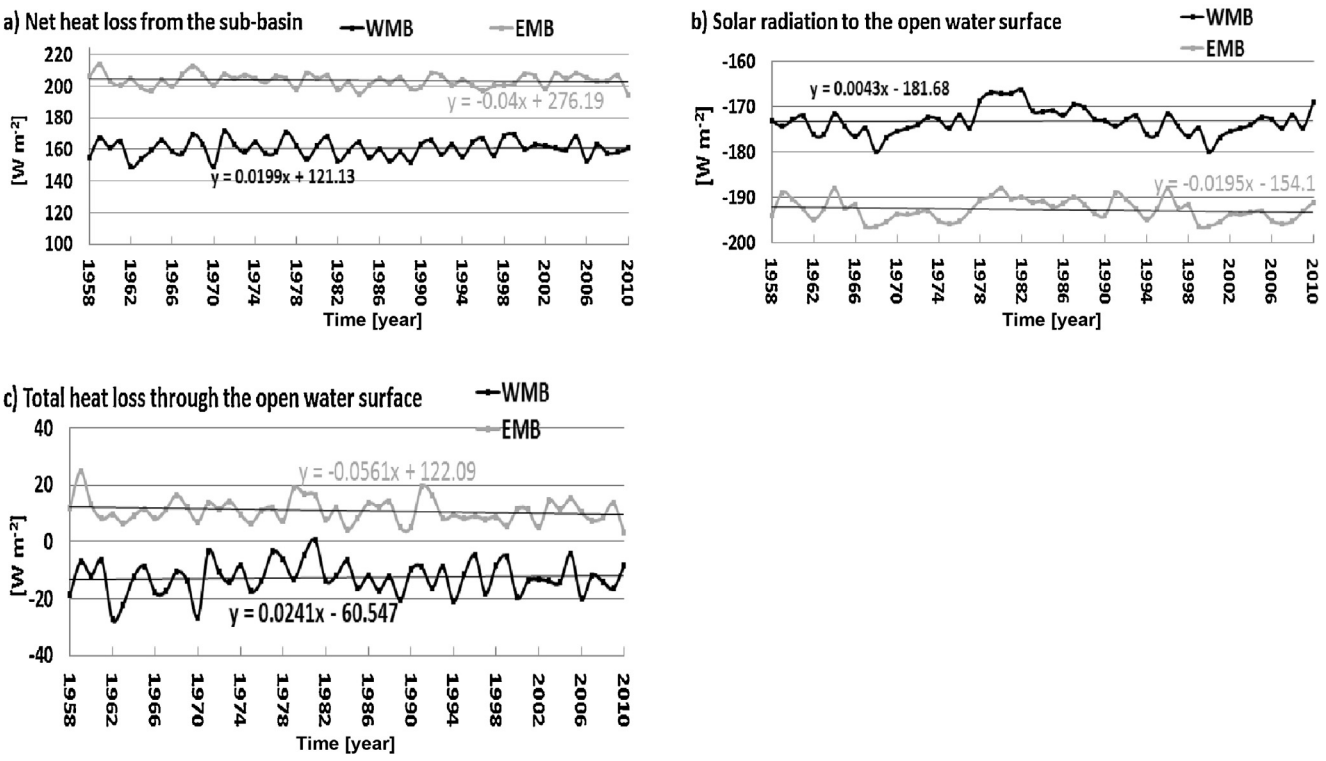

Figure 9 Annual mean modelled heat balance components for the Western and Eastern Mediterranean water components: (a) net heat loss from the sea (F_n), (b) solar radiation to the open water surface (F_s^o), and (c) total heat loss through the open water surface (F_{loss}).

4. Discussion

Similar to Shaltout and Omstedt (2012), the present work realistically reproduces the large-scale physical features of the WMB and EMB. However, several small-scale features such as deep-water convection and coastal—land interactions have not yet been included in the modelling. Instead, the present approach is based on a two-basin model that horizontally averages the sea into its western and eastern parts. Horizontal averaging reduces the effect of local features but gives an overall understanding of the water and heat balances. Based on these results, our research plan is to build a multi-basin version, PROBE-MED version 3.0 that treats the Mediterranean Sea as a number of coupled sub-basins to include local Mediterranean Sea processes. In the present version, the water exchanges through the Gibraltar Strait and Sicily Channel are calculated using a baroclinic approach. The calculated surface (lower) flow through the Gibraltar Strait averaged $0.65 \times 10^6\ m^3\ s^{-1}$ ($0.63 \times 10^6\ m^3\ s^{-1}$) annually, giving a slightly lower estimate of approximately $0.16 \times 10^6\ m^3\ s^{-1}$ than that of Soto-Navarro et al. (2010), who used the observations in calculating the flows. This is probably because the observations are not well distributed in space. Moreover, the present calculated surface flow through the Gibraltar Strait is in good agreement with the CNRM ($0.73 \times 10^6\ m^3\ s^{-1}$), MPI ($0.75 \times 10^6\ m^3\ s^{-1}$) and INGV ($0.78 \times 10^6\ m^3\ s^{-1}$) model calculations (Dubois et al., 2012). However, the present calculated surface flow is in disagreement with LMD ($0.91 \times 10^6\ m^3\ s^{-1}$) and ENEA ($1.06 \times 10^6\ m^3\ s^{-1}$) model calculations (Dubois et al., 2012). The accuracy of the present calculation of the exchange through the Gibraltar Strait was further analysed by running two sensitivity experiments. The first (second) sensitivity runs were performed by increasing the surface flow through the Gibraltar Strait by 20% (40%) of its mean value. The second sensitivity run ($Q_{in,sur,Gib} = 0.91 \times 10^6\ m^3\ s^{-1}$) indicated that the Mediterranean Sea become fresher than indicated by observations, while the first sensitivity run ($Q_{in,sur,Gib} = 0.78 \times 10^6\ m^3\ s^{-1}$) indicated no significant change in the Mediterranean Sea features compared with the current calculation. Therefore, the exchange through Gibraltar Strait seems realistic and can be addressed by the current calculation.

Moreover, the calculated surface (lower) flow through the Sicily Channel averaged $0.95 \times 10^6\ m^3\ s^{-1}$ ($0.93 \times 10^6\ m^3\ s^{-1}$) annually, giving a slightly lower estimate of approximately $0.15 \times 10^6\ m^3\ s^{-1}$ ($0.16 \times 10^6\ m^3\ s^{-1}$) than did Shaltout and Omstedt (2012). In general, the current calculated surface

Table 4 Winter correlation coefficient between NAOI and net precipitation over the Mediterranean Sea; correlations significant at a 95% significance level, n (number of observations) = 159, R = correlation coefficient.

	Western Mediterranean	Eastern Mediterranean
Precipitation	Significant $R = -0.239$	Insignificant $R = -0.051$
Evaporation	Insignificant $R = 000$	Insignificant $R = 0.049$
Net precipitation	Significant $R = -0.268$	Insignificant $R = -0.094$

water flow through the Sicily Channel agrees with the previous calculations of Astraldi et al. (1999), Bèranger et al. (2002), and Shaltout and Omstedt (2012) but disagrees with that of Molcard et al. (2002). This disagreement can be explained by the methods Molcard et al. (2002) used, which were based on the assumption of density difference.

The current study shows that there is a seasonal cycle of surface water inflow through the Gibraltar Strait (in agreement with the findings of Astraldi et al., 1999), though the surface water transport through Sicily Channel displayed no substantial seasonal difference (in agreement with the findings of Moretti et al., 1993). This is probably due to the seasonal difference (similarity) of thermohaline structure between the two sides of the Gibraltar Strait (Sicily Channel). The surface water flow through the Sicily Channel is estimated to be approximately 1.4 times the surface water flow through the Gibraltar Strait because: (1) the net evaporation over the EMB is about three times than the net evaporation over the WMB, (2) deep water convection is more significant in the EMB than the WMB, so the amount of lower-water outflow through the Sicily Channel is more significant than through the Gibraltar Strait. Depending on the two previous aspects, the amount of inflow water needed to compensate for the loss of water due to net evaporation and outflow is much higher through the Sicily Channel than the Gibraltar Strait. The Sicily Strait is 11 times wider than the Gibraltar Strait, which can explain why the surface flow through the Sicily Channel is higher than that through the Gibraltar Strait.

The calculated SST over the 1958–2010 period followed the reanalysed data with no biases over either studied sub-basin. The surface water of the EMB was approximately 1.6°C warmer than that of the WMB in the studied period. The Mediterranean Sea surface water displayed a significant warming trend, most pronounced in the 1985–2010 period and over the EMB (Table 5). The modelled sea surface salinity in the 1958–2010 period followed the reanalysed data with a bias of 0.09 and 0.11 g kg^{-1} for the WMB and EMB, respectively. The surface water of the EMB was approximately 0.87 g kg^{-1} more saline than that of the WMB. The Mediterranean Sea surface water displayed an insignificant salinity trend (Table 5). In the EMB, this can be explained by a balance between two effects: significant warming (implying increasing salinity) and decreasing freshwater input (implying decreasing salinity). The annual temperature and salinity cycles in the surface and deep layers were realistically simulated using PROBE-MED version 2.0. The calculated evaporation rate and heat balance components agreed well with and were strongly correlated with the reanalysed data. This may indicate that the air–sea interaction and turbulent mixing are modelled satisfactorily.

Table 5 shows the statistical analysis of net precipitation rates. Calculated net precipitation rates display a positive (negative) trend over the WMB (EMB), most markedly in the 1958–1984 (1985–2010) period. Moreover, the annual average net precipitation rates were -0.88 ± 0.95 and -1.52 ± 1.28 mm day^{-1} for the WMB and EMB, respectively. This may explain the much more saline surface water in the EMB than the WMB.

Different estimation methods are available for calculating net precipitation rates. ERA-Interim reanalysed data indicate that the net precipitation rates over the 1985–2010 period, calculated as long-term means, were -1.4 mm day^{-1} (trend 0.099 mm day^{-1} yr^{-1}) and -2.1 mm day^{-1} (trend -0.139 mm day^{-1} yr^{-1}) for the WMB and EMB, respectively. Romanou et al. (2010) estimated net precipitation rates for the 1988–2005 period over the Mediterranean Sea based on satellite-derived ocean fluxes (HOAPS-3). They found negative net precipitation rates of -1.1 and of -3.5 mm day^{-1} for the WMB and EMB, respectively. Mariotti et al. (2002) estimated different evaporation and precipitation rates using different datasets, and found that the Mediterranean Sea had negative net precipitation rates ranging from -1.3 to -1.9 mm day^{-1}, most markedly over EMB. The present calculations (see Table 5) and those presented in these three earlier studies thus differ only slightly.

The water balance of the Mediterranean Sea was controlled by net flow through the Gibraltar Strait and Sicily Channel, net precipitation rates, and freshwater input.

The heat balance of the Mediterranean Sea was controlled by heat loss from the water surface, solar radiation into the sea, and heat flow through the Gibraltar Strait and Sicily Channel. Both heat loss and solar radiation display significant (insignificant) trends over the EMB (EMB). This agrees with the previous findings of Shaltout and Omstedt (2012). The annual net heat gain from the WMB (-13 W m^{-2}) was balanced by the heat flow through the Gibraltar Strait and Sicily Channel. The annual net heat loss from the EMB (11 W m^{-2}) was balanced by the heat flow through the Sicily Channel.

Table 5 Trend analysis of calculated sea surface temperature, sea surface salinity, and net precipitation rates for the Western and Eastern Mediterranean sub-basins. Mean values in °C, g kg^{-1}, and mm day^{-1} for the sea surface temperature, sea surface salinity, and net precipitation rates, respectively, are also given (SD = standard deviation). The *t*-test is used to examine the significance at a 95% significance level.

Period	Sea surface temperature **Trend [°C yr^{-1}] (mean ± SD [mm day^{-1}])**		Sea surface salinity **Trend [°C yr^{-1}] (mean ± SD [g kg^{-1}])**		Net precipitation **Trend [mm day^{-1} yr^{-1}] (mean ± SD [°C])**	
	WMB	EMB	WMB	EMB	WMB	EMB
1958–2010	**Insignificant** [18.75 ± 4]	**0.16** [20.35 ± 3.8]	**Insignificant** [37.48 ± 0.13]	**Insignificant** [38.35 ± 0.16]	**0.028** [−0.88 ± 0.95]	**−0.011** [−1.52 ± 1.28]
1958–1984	**−0.37** [18.74 ± 4]	**Insignificant** [20.22 ± 3.7]	**Insignificant** [37.47 ± 0.12]	**Insignificant** [38.35 ± 0.16]	**0.196** [−0.87 ± 0.96]	**0.048** [−1.50 ± 1.29]
1985–2010	**0.40** [18.76 ± 4.1]	**0.55** [20.50 ± 3.9]	**Insignificant** [37.49 ± 0.14]	**Insignificant** [38.36 ± 0.17]	**0.102** [−0.89 ± 0.95]	**−0.040** [−1.53 ± 1.27]

References

Astraldi, M., Balopoulos, S., Candela, J., Font, J., Gacic, M., Gasparini, G.P., Manca, B., Theocharis, A., Tintoré, J., 1999. The role of straits and channels in understanding the characteristics of Mediterranean circulation. Prog. Oceanogr. 44, 65–108.

Bethoux, J.P., Durieu de Madron, X., Nyffeler, F., Tailliez, D., 2002. Deep water in the western Mediterranean: peculiar 1999 and 2000 characteristics, shelf formation hypothesis, variability since 1970 and geochemical inferences. J. Mar. Syst. 33 (34), 117–131.

Bethoux, J.P., Gentili, B., 1999. Functioning of the Mediterranean Sea: past and present changes related to freshwater input and climate changes. J. Mar. Syst. 20 (1), 33–47.

Bormans, M., Garrett, C., 1989a. The effects of rotation on the surface inflow through the strait of Gibraltar. J. Phys. Oceanogr. 19, 1535–1542.

Bormans, M., Garrett, C., 1989b. The effects of nonrectangular cross section, friction, and barotropic fluctuations on the exchange through the Strait of Gibraltar. J. Phys. Oceanogr. 19, 1543–1557.

Bèranger, K., Mortier, L., Crèpon, M., 2002. Seasonal transport variability through Gibraltar, Sicily and Corsica Straits. In: The 2nd Meeting on the Physical Oceanography of Sea Straits, Villefranche, France, 15–19 April 2002, 77–81.

Calmanti, S., Artale, V., Sutera, A., 2006. North Atlantic MOC variability and the Mediterranean Outflow: a box-model study. Tellus A 58 (3), 416–423.

Delgado, J., Garcia-Lafuente, j., Vargas, M.J., 2001. A simple model for submaximal exchange through the Strait of Gibraltar. Sci. Mar. 65 (4), 313–322.

Dubois, C., Somot, S., Calmanti, S., Carillo, A., Déqué, M., Dell' Aquilla, A., Elizalde, A., Gualdi, S., Jacob, D., L'Hévéder, B., Li, L., Oddo, P., Sannino, G., Scoccimarro, E., Sevault, F., 2012. Future projections of the surface heat and water budgets of the Mediterranean Sea in an ensemble of coupled atmosphere–ocean regional climate models. Clim. Dyn. 39, 1859–1884, http://dx.doi.org/10.1007/s00382-011-1261-4.

Edman, M., Omstedt, A., 2013. Modeling the dissolved CO_2 system in the redox environment of the Baltic Sea. Limnol. Oceanogr. 58 (1), 74–92.

Eilola, k., Gustafsson, G., Kuznetsov, I., Meier, M., Neumann, T., Savchuk, P., 2011. Evaluation of biogeochemical cycles in an ensemble of three state-of-the-art numerical models of the Baltic Sea. J. Mar. Syst. 88, 267–284, http://dx.doi.org/10.1016/j.jmarsys.2011.05.004.

Elbaz-Poulichet, F., Guieu, C., Morley, N., 2001. A reassessment of trace metal budgets in the Western Mediterranean Sea. Mar. Pollut. Bull. 42 (8), 623–627.

Garcia-Lafuente, J., Delgado, J., Criado, F., 2002. Inflow interruption by meteorological forcing in the Strait of Gibraltar. Geophys. Res. Lett. 29 (19), 1914, http://dx.doi.org/10.1029/2002GL015446.

Jakobson, E., Vihma, T., Palo, T., Jakobson, L., Keernik, H., Jaagus, J., 2012. Validation of atmospheric reanalyses over the central Arctic Ocean. Ggeophys. Res. Lett. 39, L10802, http://dx.doi.org/10.1029/2012GL051591.

Ludwig, W., Dumont, E., Meybeck, M., Heussner, S., 2009. River discharges of water and nutrients to the Mediterranean and Black Sea: major drivers for ecosystem changes during past and future decades? Prog. Oceanogr. 80 (3/4), 199–217, http://dx.doi.org/10.1016/j.pocean.2009.02.001.

Mariotti, A., Struglia, M., Zeng, N., Lau, K., 2002. The hydrological cycle in the Mediterranean region and implications for the water budget of the Mediterranean Sea. J. Clim. 15, 1674–1690, http://dx.doi.org/10.1175/1520-0442(2002)015<1674:THCITM>2.0.CO;2.

Menemenlis, D., Fukumori, I., Lee, T., 2007. Atlantic to Mediterranean Sea level difference driven by winds near Gibraltar Strait. J. Phys. Oceanogr. 37 (2), 359–376.

Malanotte-Rizzoli, P., Manca, B., d'Alcala, M., Theocharis, A., Brenner, S., Budillon, G., Ozsoy, E., 1999. The Eastern Mediterranean in the 80s and in the 90s: the big transition in the intermediate and deep circulations. Dyn. Atmos. Oceans 29 (2–4), 365–395.

Matthiesen, S., Haines, K., 2003. A hydraulic box model study of the Mediterranean response to postglacial sea-level rise. Paleoceanography 18 (4), 12.

Mertens, C., Schott, F., 1997. Interannual variability of deep-water formation in the northwestern Mediterranean. J. Phys. Oceanogr. 28, 1410–1424.

Molcard, A., Gervasio, L., Griffa, A., Gasparini, G., Mortier, L., Özgökmen, T., 2002. Numerical investigation of the Sicily Channel dynamics: density currents and water mass advection. J. Mar. Syst. 36, 219–238.

Moretti, M., Sansone, E., Spezie, G., De Maio, A., 1993. Results of investigations in the Sicily Channel (1986–1990). Deep Sea Res. II 40, 1181–1192.

Omstedt, A., 2011. Guide to Process Based Modelling of Lakes and Coastal Seas. Springer-Praxis Books in Geophysical Sciences. Springer-Verlag, Berlin/Heidelberg, http://dx.doi.org/10.1007/978-3-642-17728-6.

Omstedt, A., et al., 2014. Progress in physical oceanography of the Baltic Sea during the 2003–2014 period. Prog. Oceanogr., http://dx.doi.org/10.1016/j.pocean.2014.08.010.

Philandras, C.M., Nastos, P.T., Kapsomenakis, J., Douvis, K.C., Tselioudis, G., Zerefos, C.S., 2011. Long term precipitation trends and variability within the Mediterranean region. Nat. Hazards Earth Syst. Sci. 11, 3235–3250, http://dx.doi.org/10.5194/nhess-11-3235-201.

Pierini, S., Rubino, A., 2001. Modeling the oceanic circulation in the area of the Strait of Sicily: the remotely forced dynamics. J. Phys. Oceanogr. 31, 1397–1412.

Rixen, J., Beckers, M., Levitus, S., Antonov, J., Boyer, T., Maillard, C., Fichaut, M., Balopoulos, E., Iona, S., Dooley, H., Garca, M.J., Manca, B., Giorgetti, A., Manzella, G., Mikhailov, N., Pinardi, N., Zavatarelli, M., 2005. The Western Mediterranean deep water: a proxy for climate change. Geophys. Res. Lett. 32, L12608, http://dx.doi.org/10.1029/2005GL022702.

Romanou, A., Tselioudis, G., Zerefos, C., Clayson, C., Curry, J., Andersson, A., 2010. Evaporation–precipitation variability over the Mediterranean and the Black Seas from satellite and reanalysis estimates. J. Clim. 23 (19), 5268–5287, http://dx.doi.org/10.1175/2010JCLI3525.1.

Salat, J., Font, J., 1987. Water mass structure near and offshore the Catalan coast during winters of 1982 and 1983. Ann. Geophys. 5B (1), 49–54.

Shaltout, M., Omstedt, A., 2012. Calculating the water and heat balances of the Eastern Mediterranean Basin using ocean modelling and available meteorological, hydrological and ocean data. Oceanologia 54 (2), 199–232.

Shaltout, M., Omstedt, A., 2014. Recent dynamic topography changes in the Mediterranean Sea analysed from satellite altimetry data. Curr. Dev. Oceanogr. (in press).

Skliris, N., Sofianos, S., Lascaratos, A., 2007. Hydrological changes in the Mediterranean Sea in relation to changes in the freshwater budget: a numerical modelling study. J. Mar. Syst. 65 (1–4), 400–416.

Soto-Navarro, J., Criado-Aldeanueva, F., García-Lafuente, J., Sánchez-Román, A., 2010. Estimation of the Atlantic inflow through the Strait of Gibraltar from climatological and in situ data. J. Geophys. Res. 115, C10023, http://dx.doi.org/10.1029/2010JC006302.

Sparnocchia, S., Picco, P., Manzella, G.M.R., Ribotti, A., Copello, S., Brasey, P., 1995. Intermediate water formation in the Ligurian Sea. Oceanol. Acta 18 (2), 151–162.

Stanev, E., Peneva, E.L., 2002. Regional sea level response to global climatic change: Black Sea examples. Global Planet. Change 32 (1), 33–47.

Stansfield, K., Smeed, D.A., Gasparini, G.P., 2002. The path of the overflows from the sills in the Sicily Strait. In: The 2nd Meeting on the Physical Oceanography of Sea Straits, Villefranche, France, 15—19 April 2002, 211—215.

Stigebrandt, A., 2001. Physical oceanography of the Baltic Sea. Ecological studies. In: Wulff, E., et al. (Eds.), A System Analysis of the Baltic Sea, vol. 148. Springer-Verlag, Berlin, 19—74.

Stow, C., Jolliff, J., McGillicuddy, D., Doney, S., Allen, J., Friedrichs, M., Rose, K., Wallhead, P., 2009. Skill assessment for coupled biological/physical models of marine systems. J. Mar. Syst. 76, 4—15, http://dx.doi.org/10.1016/j.jmarsys.2008.03.011.

Tsimplis, M.N., Bryden, H.L., 2000. Estimating of the transport through the strait of Gibraltar. Deep Sea Res. 47, 2219—2242.

Tsimplis, M.N., Josey, S.A., 2001. Forcing of the Mediterranean sea by atmospheric oscillation over the north Atlantic. Geophys. Res. Lett. 28, 803—806.

Tziperman, E., Speer, K., 1994. A study of water mass transformation in the Mediterranean Sea: analysis of climatological data and a simple three-box model. Dyn. Atmos. Oceans 21 (2), 53—82.

Zervakis, V., Georgopoulos, D., Drakopoulos, P., 2000. The role of the North Aegean in triggering the recent Eastern Mediterranean climatic changes. J. Geophys. Res. 105 (C11), 26103—26116.